Models of IP_3 and Ca^{2+} Oscillations: Frequency Encoding and Identification of Underlying Feedbacks

Antonio Politi,* Lawrence D. Gaspers,† Andrew P. Thomas,† and Thomas Höfer*
*Department of Theoretical Biophysics, Institute of Biology, Humboldt University Berlin, 10115 Berlin, Germany; and
†Department of Physiology and Pharmacology, University of Medicine and Dentistry of New Jersey, Newark, New Jersey

ABSTRACT Hormones that act through the calcium-releasing messenger, inositol 1,4,5-trisphosphate (IP_3), cause intracellular calcium oscillations, which have been ascribed to calcium feedbacks on the IP_3 receptor. Recent studies have shown that IP_3 levels oscillate together with the cytoplasmic calcium concentration. To investigate the functional significance of this phenomenon, we have developed mathematical models of the interaction of both second messengers. The models account for both positive and negative feedbacks of calcium on IP_3 metabolism, mediated by calcium activation of phospholipase C and IP_3 3-kinase, respectively. The coupled IP_3 and calcium oscillations have a greatly expanded frequency range compared to calcium fluctuations obtained with clamped IP_3. Therefore the feedbacks can be physiologically important in supporting the efficient frequency encoding of hormone concentration observed in many cell types. This action of the feedbacks depends on the turnover rate of IP_3. To shape the oscillations, positive feedback requires fast IP_3 turnover, whereas negative feedback requires slow IP_3 turnover. The ectopic expression of an IP_3 binding protein has been used to decrease the rate of IP_3 turnover experimentally, resulting in a dose-dependent slowing and eventual quenching of the Ca^{2+} oscillations. These results are consistent with a model based on positive feedback of Ca^{2+} on IP_3 production.

INTRODUCTION

The release of Ca^{2+} ions from intracellular stores is a central event in the transduction of hormone and neurotransmitter signals. In a multitude of cell types, the activation of receptors coupled to the phosphoinositide pathway triggers oscillations in the cytoplasmic Ca^{2+} concentration ($[Ca^{2+}]_c$). In many cell types, the strength of the extracellular stimulus is encoded primarily in the frequency of the $[Ca^{2+}]_c$ oscillations, which increases with the degree of stimulation. For example, in rat hepatocytes, the periods of $[Ca^{2+}]_c$ oscillations range over one order of magnitude, from >250 s for low concentrations of hormones, such as vasopressin and noradrenalin, to ~30 s for higher hormone doses (1).

A long-standing question has been whether the oscillations are generated by the cellular Ca^{2+} transporters and channels themselves or whether they originate upstream in the signal transduction machinery, between hormone binding to its receptor and the activation of Ca^{2+} fluxes. It has been proposed that the periodic release of Ca^{2+} ions from the endoplasmic reticulum (ER) can be brought about through the regulatory properties of the IP_3 receptor (IP_3R), the main type of ER calcium release channel in nonexcitable cells (2–5). Mathematical models have demonstrated how fast activation and delayed inhibition of the IP_3R by cytoplasmic Ca^{2+} can drive repetitive Ca^{2+} spiking (6–8). In these models, IP_3 is required to initially open the IP_3R and sensitize the channel toward feedback activation by cytoplasmic calcium. Therefore, Ca^{2+} oscillations can occur when IP_3 concentration is held at a constant value. However, models based on a simple description of the IP_3R dynamics generally produce $[Ca^{2+}]_c$ oscillations with short periods (~10–60 s) and thus do not reproduce the long interspike intervals observed experimentally. Long-period oscillations have been obtained when additional mechanisms, such as the regulation of IP_3R by phosphorylation, stochastic gating phenomena or slow calcium buffers, are included (9,10,11).

Recently, it has become possible to monitor IP_3 changes in intact cells. These experiments have shown that, for some of the agonists used, the IP_3 concentration is highly dynamic and can oscillate together with cytoplasmic calcium (12–15). This raises the intriguing possibility that a coupled IP_3-Ca^{2+} oscillator may generate long-period oscillations and underlie the efficient frequency encoding of the hormone dose.

The existence of both positive and negative feedbacks of Ca^{2+} on IP_3 metabolism could mediate fluctuations in cellular IP_3 levels. The production of IP_3 is catalyzed by a diverse family of phosphoinositide-specific phospholipase C (PLC) isoforms (16). All PLC isoforms are activated by Ca^{2+} ions, although their sensitivities to $[Ca^{2+}]$ vary greatly (17,18). This feedback can have an important role in Ca^{2+} wave propagation (19–22). IP_3 is removed by phosphorylation or dephosphorylation through IP_3 3-kinase (IP_3K) or IP_3 5-phosphatase (IP_3P), respectively. IP_3 removal by IP_3K is activated by Ca^{2+} (23–25). Moreover, it has also been suggested that protein kinase C (PKC), which is activated by receptor-mediated increases in Ca^{2+} and diacylglycerol, may inhibit IP_3 production by inactivating agonist receptors (13,26). However, it is presently not clear what

Submitted August 29, 2005, and accepted for publication January 25, 2006.

Antonio Politi and Lawrence D. Gaspers contributed equally to this work.
Address reprint requests to Thomas Höfer, Dept. of Theoretical Biophysics, Institute of Biology, Humboldt University Berlin, Invalidenstrasse 42, 10115 Berlin, Germany. Tel.: 4930-2093-8592-8698; Fax: 4930-2093-8813; E-mail: thomas.hoefer@biologie.hu-berlin.de.

0006-3495/06/05/3120/14 $2.00
doi: 10.1529/biophysj.105.072249

effects such feedbacks have on Ca^{2+} oscillations. Importantly, it is not known whether the involvement of these Ca^{2+}-dependent feedback mechanisms serves a physiological role.

Previous models have shown that IP_3-mediated Ca^{2+} release coupled to Ca^{2+}-activated PLC can generate oscillations, without any requirement of IP_3R regulation by Ca^{2+} (26,27). These models have been criticized because in some cell types Ca^{2+} oscillations can also be elicited by IP_3 or its nonmetabolizable analogs (3,28,29). The incorporation of Ca^{2+} activation of PLC into a Ca^{2+} oscillator model based on the above-described IP_3R properties has been reported to modulate Ca^{2+} oscillations (30), whereas the inclusion of IP_3K has been found to have practically no effect (31,32).

In this work, we have carried out a systematic modeling study of the interaction between cellular Ca^{2+} transports and IP_3 metabolism. The model includes the dynamics of IP_3, Ca^{2+}, and IP_3R and takes into account positive and negative feedback of Ca^{2+} on the IP_3 metabolism. These are mediated by Ca^{2+} activation of IP_3 generation through PLC and Ca^{2+} activation of IP_3 removal by IP_3K, respectively. We have found that each of these Ca^{2+} feedbacks strongly modifies the properties of a core oscillator based on Ca^{2+} and IP_3R dynamics and, in particular, substantially expands the range of oscillation frequencies. Thus IP_3 oscillations may underlie efficient frequency encoding of the hormone signal. The model analysis shows that the lifetime of IP_3 is a critical parameter in the system, the experimental perturbation of which can give information on the feedbacks present. We directly tested this theory in Chinese hamster ovary (CHO) cells by transiently expressing an IP_3 binding protein composed of the N-terminal ligand-binding domain of the type 1 IP_3R fused to green fluorescent protein. The overexpression of this fusion protein exerted a dose-dependent suppression of repetitive agonist-induced Ca^{2+} oscillations that is consistent with an oscillator model including positive feedback of Ca^{2+} on IP_3 generation. Taken together, the experimental data and theoretical analysis suggest that IP_3 oscillations are an essential component of the Ca^{2+} oscillator, expanding the richness in the message conveyed by extracellular stimuli.

MATERIALS AND METHODS

Mathematical model

The model accounts for the formation and degradation of IP_3, the main Ca^{2+} fluxes across the ER and plasma membrane, and the IP_3R dynamics (see Fig. 1). It is formulated in terms of four variables: the IP_3 and Ca^{2+} concentrations in the cytoplasm, p and c, respectively; the calcium concentration in the ER stores, s; and the fraction of IP_3R that have not been inactivated by Ca^{2+}, r.

IP_3 dynamics

IP_3 is produced by PLC, whose activity depends on agonist dose and Ca^{2+}. The Ca^{2+} sensitivity of PLCβ can be modeled by (33)

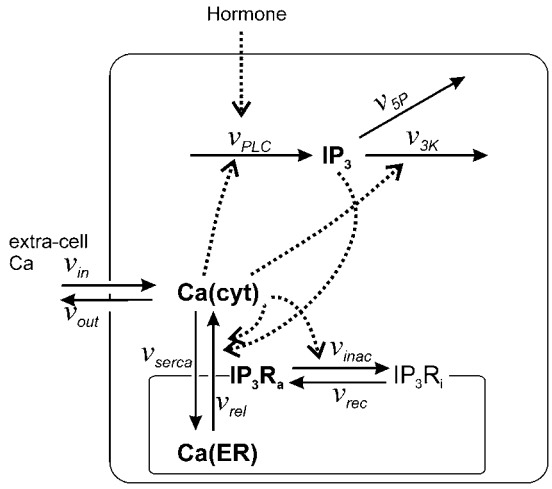

FIGURE 1 Interactions between Ca^{2+} transport processes and IP_3 metabolism included in the model. The solid and dashed arrows indicate transport/reaction steps and activations, respectively. The bold quantities indicate the model variables: IP_3, cytoplasmic IP_3; Ca(cyt), free cytoplasmic Ca^{2+}; Ca(ER), free Ca^{2+} in the ER; IP_3R_a, active conformation of the IP_3R. The other abbreviations denote: IP_3R_i, inactive conformation of the IP_3R; v_{rel}, rate of Ca^{2+} release through the IP_3R; v_{serca}, active Ca^{2+} transport into the ER; v_{ina} and v_{rec} rate of Ca^{2+}-induced IP_3R inactivation and recovery rate, respectively; v_{PLC}, production rate of IP_3; v_{5P} and v_{3K} rates of IP_3 dephosphorylation and phosphorylation, respectively; v_{in} and v_{out}, rates of Ca^{2+} influx and extrusion across the plasma membrane, respectively.

$$v_{\mathrm{PLC}} = V_{\mathrm{PLC}}\frac{c^2}{K_{\mathrm{PLC}}^2 + c^2}. \tag{1}$$

The maximal rate V_{PLC} depends on the agonist concentration, whereas K_{PLC} characterizes the sensitivity of PLC to Ca^{2+}. IP_3 is removed through dephosphorylation by IP_3P and phosphorylation by IP_3K, which we model as

$$v_{\mathrm{deg}} = v_{5\mathrm{P}} + v_{3\mathrm{K}} = \left(k_{5\mathrm{P}} + k_{3\mathrm{K}}\frac{c^2}{K_{3\mathrm{K}}^2 + c^2}\right)p, \tag{2}$$

where k_{5P} and k_{3K} are the IP_3 dephosphorylation and phosphorylation rate constants, respectively. The Ca^{2+} dependence of the IP_3K is described by a Hill function with the half-saturation constant K_{3K} (23). According to Fink et al. (34) and Sims and Allbritton (35), one can assume that the two enzymes are not saturated with IP_3, justifying the linear rate law in p.

For the purpose of the subsequent analysis we write the balance equation for the IP_3 concentration in the following form

$$\begin{aligned}\frac{dp}{dt} &= v_{\mathrm{PLC}} - v_{\mathrm{deg}} \\ &= \frac{1}{\tau_{\mathrm{p}}}\left[\bar{V}_{\mathrm{PLC}}\frac{c^2}{K_{\mathrm{PLC}}^2 + c^2} - \left(\eta\frac{c^2}{K_{3\mathrm{K}}^2 + c^2} - (1-\eta)\right)p\right],\end{aligned} \tag{3}$$

where we introduce the characteristic time of IP_3 turnover

$$\tau_{\mathrm{p}} = 1/(k_{3\mathrm{K}} + k_{5\mathrm{P}}), \tag{4}$$

and the ratio of the maximal IP_3K rate to the total maximal degradation rate of IP_3

$$\eta = k_{3\mathrm{K}}/(k_{3\mathrm{K}} + k_{5\mathrm{P}}). \tag{5}$$

The strength of the positive feedback will be tuned by changing K_{PLC} (the Ca^{2+} sensitivity of PLC), and the strength of the negative feedback will be

tuned by changing η (the relative expression level of IP_3K). Although both feedbacks can be present simultaneously, it is useful to first analyze them separately. Therefore, we define the ''positive-feedback model'' in which PLC is sensitive to Ca^{2+} ($K_{PLC}>0$) and IP_3K is not expressed ($\eta = 0$), and the ''negative-feedback model'' in which IP_3K is present ($\eta > 0$) and PLC is assumed insensitive to physiological Ca^{2+} changes ($K_{PLC} = 0$).

Note that the rescaled maximal PLC activity $\bar{V}_{PLC} = V_{PLC}\,\tau_p$ equals the steady-state concentration of IP_3 that would be attained in the absence of positive or negative feedbacks.

Calcium and IP_3R dynamics

The Ca^{2+} release flux through the IP_3R, v_{rel}, is modeled according to Li and Rinzel (36). The rate equations for active transport of Ca^{2+} across the ER and plasma membranes, v_{serca} and v_{out}, respectively, follow Lytton et al. (37) and Camello et al. (38). Calcium influx v_{in} includes a leak into the cell and a stimulation dependent influx. The balance equation for cytoplasmic Ca^{2+} then reads

$$\frac{dc}{dt} = \underbrace{\left(k_1\left(r\frac{c}{K_a + c}\frac{p}{K_p + p}\right)^3 + k_2\right)(s-c)}_{v_{rel}} - \underbrace{V_{serca}\frac{c^2}{K_{serca}^2 + c^2}}_{v_{serca}} + \underbrace{\varepsilon\left(v_0 + \phi\bar{V}_{PLC} - V_{pm}\frac{c^2}{K_{pm}^2 + c^2}\right)}_{v_{in} - v_{out}}. \quad (6)$$

The dimensionless parameter ε measures the relative strength of the plasma membrane fluxes, which is known to be cell-type specific. We first carry out the model analysis for the simpler case that the plasma membrane fluxes are negligible. Setting $\varepsilon = 0$ the total Ca^{2+} concentration in the cell is conserved and can be expressed as $c_{tot} = c + \beta s$, where β is the ratio of effective cytoplasmic volume to effective ER volume (both accounting for Ca^{2+} buffering). Therefore, we can insert for the ER calcium in Eq. 6, $s = (c_{tot} - c)/\beta$. In the presence of plasma-membrane fluxes ($\varepsilon > 0$) this conservation no longer holds and a kinetic equation for s must be added:

$$\frac{ds}{dt} = \frac{1}{\beta}\left[V_{serca}\frac{c^2}{K_{serca}^2 + c^2} - \left(k_1\left(r\frac{c}{K_a + c}\frac{p}{K_p + p}\right)^3 + k_2\right)(s-c)\right]. \quad (7)$$

The dynamics of IP_3R inactivation by cytoplasmic Ca^{2+} is described by (35)

$$\frac{dr}{dt} = v_{rec} - v_{inac} = \frac{1}{\tau_r}\left(1 - r\frac{K_i + c}{K_i}\right). \quad (8)$$

The meaning and numerical values of the kinetic parameters are given in Table 1.

Numerical solutions of the differential equations system, Eqs. 3 and 6–8, were obtained using a fourth-order Runge-Kutta algorithm implemented in XPPAUT (http://www.math.pitt.edu/~bard/xpp/xpp.html). Bifurcation analyses were done using the program AUTO2000 (39). Calcium waves with the local kinetics given by Eqs. 3 and 6–8 and diffusion of Ca^{2+} and IP_3 were calculated numerically with a finite-difference Crank-Nicholson scheme. Wave speeds for solitary waves were evaluated using AUTO2000.

TABLE 1 Reference parameter values

	Positive feedback	Negative feedback
IP_3 dynamics parameters		
Half-activation constant of IP_3K, K_{3K}	0.4 μM	0.4 μM
IP_3 phosphorylation rate constant, k_{3K}	0	0.1 s^{-1}
IP_3 dephosphorylation rate constant, k_{5P}	0.66 s^{-1}	0
Half-activation constant of PLC, K_{PLC}	0.2 μM	0 μM
Ca^{2+} transport and structural parameters		
Ratio of effective volumes ER/cytosol, β	0.185	0.185
Maximal SERCA pump rate, V_{serca}	0.9 μM s^{-1}	0.25 μM s^{-1}
Half-activation constant, K_{serca}	0.1 μM	0.1 μM
Maximal PMCA pump rate, V_{pm}	0.01 μM s^{-1}	0.01 μM s^{-1}
Half-activation constant, K_{pm}	0.12 μM	0.12 μM
Constant influx, v_0	0.0004 μM/s	0.0004 μM/s
Stimulation-dependent influx, ϕ	0.0047 s^{-1}	0.045 s^{-1}
Strength of plasma membrane fluxes, ε	0	0
Total Ca^{2+} concentration (for $\varepsilon = 0$), c_{tot}	2 μM	2 μM
IP_3R parameters		
Maximal rate of Ca^{2+} release, k_1	1.11 s^{-1}	7.4 s^{-1}
Ca^{2+} leak, k_2	0.0203 s^{-1}	0.00148 s^{-1}
Ca^{2+} binding to activating site, K_a	0.08 μM	0.2 μM
Ca^{2+} binding to inhibiting site, K_i	0.4 μM	0.3 μM
IP_3 binding, K_p	0.13 μM	0.13 μM
Characteristic time IP_3R inactivation, τ_R	12.5 s	6.6 s

The half-saturation constants for PLC and IP_3K were taken from Blank et al. (32) and Communi et al. (22), respectively. The IP_3 degradation rate constants were chosen in accordance to Fink et al. (33) and Sims and Allbritton (34). The maximal rate of PLC, V_{PLC}, is taken as the stimulation-dependent control parameter. In the positive-feedback model (Ca^{2+} activation of PLC), the parameters for the Ca^{2+} transport processes and the IP_3R were taken from Li and Rinzel (35). In the negative feedback model (Ca^{2+} activation of IP_3K), we obtained no substantial effect of the IP_3K on the oscillations with these parameters. However, for different parameters (as given) the IP_3K effects were pronounced. The differences in the Ca^{2+} fluxes between the two models can be accounted for by variations in the expression of the involved proteins. The differences in the Ca^{2+} binding properties to the activating site of the IP_3R can be due to differences in the expression of IP_3R subtypes, with IP_3R subtype I having a higher Ca^{2+} dissociation constant for the activating site than subtypes II and III (52,53). The table gives the reference parameter set; parameters that are varied in specific simulations are indicated in the respective figure legends.

Experimental procedures

Cell culture

CHO cells were cultured in Ham's F-12 media supplemented with 10% fetal bovine serum (FBS) and antibiotics. Cells were seeded onto poly-D-lysine coated glass coverslips (25 mm) and maintained in culture until 70–80% confluent before experimental protocols.

Plasmid construction and transfection protocols

The cDNA encoding 620 amino acids of the N-terminal rat type 1 IP_3 receptor (40) was ligated in-frame to the C-terminus of the enhanced green fluorescent protein gene in the plasmid pEGFP-C1 (Clontech, Palo Alto, CA) to generate the plasmid pEGFP-LBD. Cell cultures were transiently transfected with either pEGFP-LBD (EGFP-LBD) or pEGFP-C1 (EGFP) using Lipofectamine 2000 (Invitrogen, Carlsbad, CA) according to the manufacturer's protocols. Agonist-evoked $[Ca^{2+}]_c$ responses were recorded in transfected cultures after a 16–48-h incubation period.

Imaging measurements of $[Ca^{2+}]_c$ and fluorescent proteins

Calcium imaging experiments were performed in a HEPES-buffered physiological saline solution (HBSS) comprising (in mM): 25 HEPES (pH 7.4 at 37°C), 121 NaCl, 5 $NaHCO_3$, 4.7 KCl, 1.2 KH_2PO_4, 1.2 $MgSO_4$,

2.0 $CaCl_2$, 10 glucose, 0.1 sulphobromophthalein, and 0.25% (w/v) fatty acid-free BSA. Cell cultures were loaded with fura-2/AM by incubation with 5 μM fura-2/AM plus Pluronic F-127 (0.02% v/v) for 20–40 min in HBSS. The cells were washed and transferred to a thermostatically regulated microscope chamber (37°C). Fura-2 fluorescence images (excitation, 340 and 380 nm, emission 420–600 nm) were acquired at 3–4-s intervals with a cooled charge-coupled device (CCD) camera as previously described (3). Fura-2 fluorescence intensities were corrected for GFP spillover before calculating fluorescence ratio values, by quenching cytosolic fura-2 with $MnCl_2$. Cells expressing recombinant proteins were selected by screening for GFP fluorescence (excitation 488 nm, emission 525 nm).

EGFP-LBD concentration was estimated from a standard curve constructed with known concentrations of six His-tagged EGFP (Clontech; molecular weight of 27,000). Calibration solutions were prepared by diluting the recombinant protein in PBS. An aliquot (5 μl) was mixed with low-density mineral oil then sandwiched between two glass coverslips. EGFP containing ''bubbles'' ranging in size from 10 to 50 μm (the approximate range of cell diameters observed in CHO cultures) were imaged with a Nikon 20×, 0.75 NA Plan Apo objective on a wide-field microscope. The fluorophore protein concentration was converted into molar value assuming a molecular weight of 27,000 for His-tagged EGFP.

RESULTS

Positive and negative feedback models exhibit frequency encoding of agonist dose

In many cell types, one observes a strong dependence of the frequency of Ca^{2+} oscillations on the dose of the applied receptor agonist, whereas the oscillation amplitude remains nearly constant (1). A stepwise increase of the agonist concentration is accompanied by a prompt rise of the oscillation frequency. In the model, the maximal rate of PLC, V_{PLC}, is a measure of agonist concentration. We subjected the positive-feedback model, with Ca^{2+} activation of PLC, and the negative-feedback model, with Ca^{2+} activation of IP_3K, to stepwise increases in V_{PLC}. The responses are shown in Fig. 2, *A* and *B*, respectively, with the time points of V_{PLC} increase indicated by arrowheads. Both models exhibit a large range of oscillation frequencies with little change in $[Ca^{2+}]_c$ amplitude (Fig. 2, *A* and *B*; *top traces*). The pronounced increase in the rate of spiking with increasing stimulus is the hallmark of the experimentally observed frequency encoding. For very large stimuli, a plateau of elevated $[Ca^{2+}]_c$ is reached, again in agreement with experimental data.

The $[Ca^{2+}]_c$ oscillations in both models consist of a series of sharp spikes with baseline interludes (Fig. 2, *A* and *B*). The peak values of $[Ca^{2+}]_c$ and $[IP_3]$ occur nearly at the same time. The shape of the $[IP_3]$ oscillations in the two models is different. In the positive-feedback model, $[IP_3]$ exhibits baseline-separated spikes (Fig. 2 *A*). In contrast, in the negative-feedback model, $[IP_3]$ follows a zig-zag pattern: the occurrence of a $[Ca^{2+}]_c$ spike leads to an abrupt decrease in $[IP_3]$, after which $[IP_3]$ slowly builds up again over the whole oscillation period (Fig. 2 *B*). The IP_3R activities show similar dynamics in both models.

The behavior of the two model systems for different stimulation strengths can be summarized in bifurcation diagrams (Fig. 2, *C* and *D*). We computed the steady states of $[Ca^{2+}]_c$ and the maxima and minima of $[Ca^{2+}]_c$ oscillations as a function of V_{PLC}. For very low PLC activity, both models show a stable steady state of low $[Ca^{2+}]_c$; similarly, an elevated

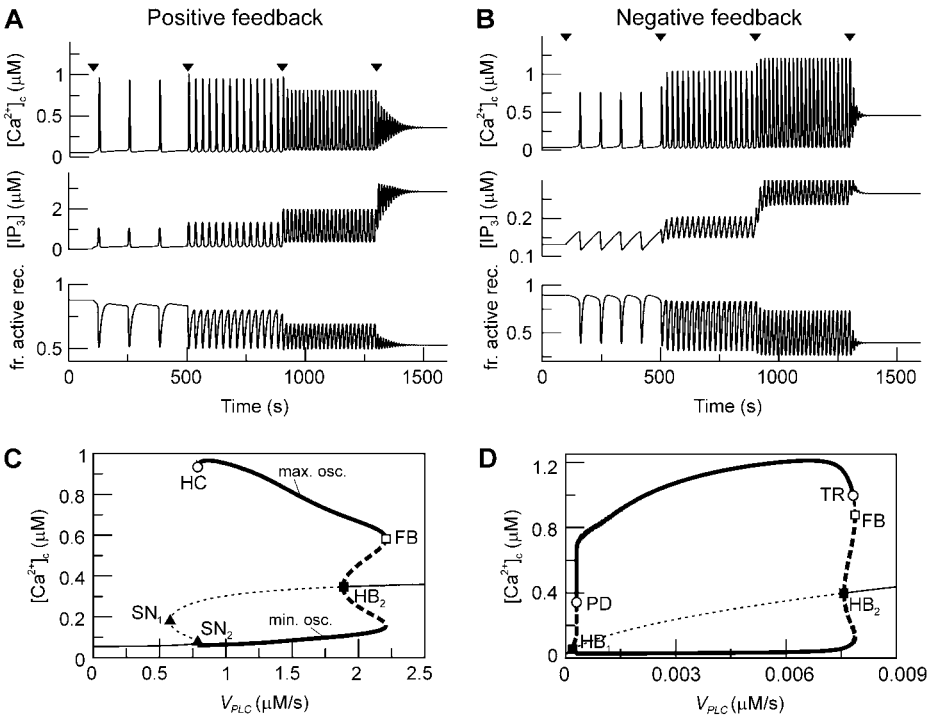

FIGURE 2 Agonist-induced IP_3 and Ca^{2+} oscillations in the positive and negative feedback models. (*A*) Positive feedback model with Ca^{2+} activation of PLC. Changes in $[Ca^{2+}]_c$, $[IP_3]$, and in the fraction of active receptors r (*top*, *middle*, and *bottom panels*) after stepwise increases in the agonist concentration (*arrowheads*), modeled by an increase in the maximal rate of PLC ($V_{PLC} = 0.3$ μM/s for $t < 100$ with successive increases to 0.787, 1, 1.5, and 2.5 μM/s). (*B*) Negative feedback model with Ca^{2+} activation of IP_3K. The response is shown for a step protocol with $V_{PLC} = 0.1$ nM/s for $t < 100$, followed by increases to 0.45, 2.5, 5.8, and 10 nM/s. (*C*) Bifurcation diagram for positive feedback model; shown are the maxima and minima of the $[Ca^{2+}]_c$ oscillations (*thick lines*) and the $[Ca^{2+}]_c$ steady states (*thin lines*) as a function of the stimulus (V_{PLC}). Solid and dashed lines indicate stable and unstable states, respectively. HB, Hopf bifurcation; HC, homoclinic bifurcation; SN, saddle-node bifurcation; FB, saddle node of periodics. (*D*) Bifurcation diagram for negative feedback model. PD, period doubling; TR, torus bifurcation. Between PD and HB_1 and TR and FB there exist complex oscillations (omitted for clarity). The parameter values used are listed in Table 1.

$[Ca^{2+}]_c$ plateau is reached at relatively high PLC activity (these stable steady states are indicated by *thin solid lines*). For an intermediate range of V_{PLC}, the steady states are unstable (*thin dashed lines*). In these regions, both models exhibit oscillations ($[Ca^{2+}]_c$ maxima and minima in stable oscillations are depicted by *thick solid lines*). The oscillations arise either via Hopf bifurcations (HB), or, in the case of the positive-feedback model, also by a homoclinic bifurcation (HC).

Further bifurcations are indicated and referred to in the figure legend. In particular, a homoclinic bifurcation is associated with the existence of multiple steady states, which arise through saddle-node bifurcations (Fig. 2 *C*, *SN*). Such multistationarity is typical for models that neglect the plasma-membrane fluxes of calcium; this point will be discussed in more detail below. In the negative-feedback model, there are two regions near the Hopf bifurcations HB_1 and HB_2 (before the point *PD* and after the point *TR* in Fig. 2 *D*) where irregular and bursting oscillations are observed (results not shown). Because these two regions are extremely narrow, compared to the total stimulation range in the negative feedback model, our focus will be on the regular oscillations.

In the two bifurcation diagrams, one notices that the V_{PLC} values required for oscillations are considerably smaller in the negative-feedback model than in the positive-feedback model. This is primarily a consequence of the different feedback mechanisms. First, in the positive-feedback model the actual PLC activity is Ca^{2+} dependent and, therefore, is lower than V_{PLC} at resting $[Ca^{2+}]_c$. Second, owing to the calcium activation of IP_3K in the negative-feedback model, the IP_3 degradation rate at resting $[Ca^{2+}]_c$ is much smaller than in the positive-feedback model, requiring a smaller rate of IP_3 production to raise $[IP_3]$ and induce oscillations.

The wide range of oscillation periods is due to interactions of IP_3 and Ca^{2+} dynamics

To elucidate whether the IP_3 dynamics participate in frequency encoding, we compared the oscillation periods in models without any Ca^{2+} feedback on IP_3 (resulting in a constant $[IP_3]$) and in the two feedback models (with $[IP_3]$ oscillations).

We begin by discussing the positive-feedback model. In the positive-feedback model, we consider Ca^{2+} activation of the agonist-dependent PLCβ. The strength of the positive feedback can be tuned by changing the value of the Ca^{2+} activation constant, K_{PLC}. For K_{PLC} being much lower than the basal $[Ca^{2+}]_c$, PLC is always saturated with Ca^{2+} and its activity is independent of variations in $[Ca^{2+}]_c$. In particular, by setting $K_{PLC} = 0$ positive feedback will effectively be eliminated. This model with constant $[IP_3]$ shows fast calcium oscillations with a period of 10–15 s (Fig. 3 *A*, *dashed line*). Introducing positive feedback by setting $K_{PLC} > 0$ causes oscillations with long periods at low stimulation. The frequency encoding of the stimulus becomes very pronounced when the sensitivity of PLC to changes in $[Ca^{2+}]_c$ is

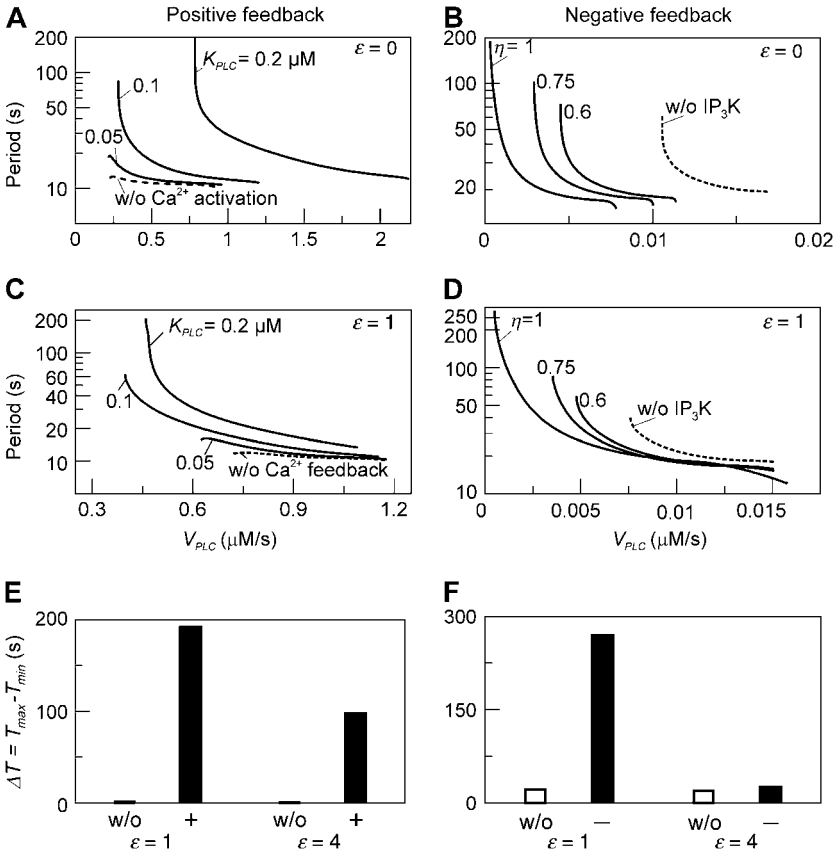

FIGURE 3 Frequency encoding of agonist stimulus. (*A*) Positive feedback: oscillation periods observed at different stimulation strengths (varying V_{PLC}). Increasing the half-saturation constant of PLC for Ca^{2+}, K_{PLC}, from 0 (no functional positive feedback) to 0.2 μM (functional feedback) greatly enhances frequency encoding. (*B*) Negative feedback. Increasing the amount of IP_3K relative to IP_3P (η) enhances frequency encoding. (*C*, *D*) The feedback effects shown in panels *A* and *B* are preserved when plasma-membrane fluxes of Ca^{2+} are included in the models ($\varepsilon = 1$). (*E*) Range of oscillation periods, $\Delta T = T_{max} - T_{min}$, in the presence (+) and absence (w/o) of positive feedback for two different strengths of the plasma-membrane Ca^{2+} fluxes ($\varepsilon = 1, 4$). (*F*) Range of oscillation periods in the presence (−) and absence (w/o) of negative feedback for two different strengths of the plasma-membrane Ca^{2+} fluxes ($\varepsilon = 1, 4$). We have found that the IP_3K has an impact on the oscillation period only when the Ca^{2+} fluxes between ER and cytoplasm are comparatively slow and the IP_3R is less sensitive to Ca^{2+} activation. To expose the period effect of the negative feedback, we have chosen different parameter values than in the positive feedback model (see Table 1).

just above basal $[Ca^{2+}]_c$ (Fig. 3 *A*, *solid lines*; $K_{PLC} = 0.1$ and 0.2 μM).

For the negative-feedback model, we recall that there are two removal pathways for IP_3, one catalyzed by the Ca^{2+}-insensitive IP_3 5-phosphatase (IP_3P) and the other by the Ca^{2+}-activated IP_3 3-kinase (IP_3K). We can modify the strength of the negative feedback by taking different concentration ratios of IP_3P and IP_3K. The feedback strength is expressed by the ratio of the maximal IP_3K rate to the total degradation rate of IP_3; $\eta = k_{3K}/(k_{3K} + k_{5P})$, where $k_{3K} + k_{5P}$ has been kept constant in the following calculations. The oscillation periods in the absence of negative feedback ($\eta = 0$), and therefore constant $[IP_3]$, are shown in Fig. 3 *B* (*dashed line*). When η is sufficiently high, the negative feedback has a pronounced effect on the range of oscillations periods; for $\eta \geq 0.6$ there is an increase in the period range (Fig. 3 *B*, *solid lines*).

In the positive-feedback model, arbitrarily long periods can be obtained (exceeding the 200 s shown), which are due to the onset of the oscillations via a homoclinic bifurcation (see also Fig. 2 *C*). The homoclinic bifurcation specifically occurs in the model when the plasma-membrane fluxes of Ca^{2+} are neglected, which is a valid simplification for many cell types in which the contribution of these fluxes to Ca^{2+} oscillations is small (41). We have also studied the more general case when the plasma-membrane Ca^{2+} fluxes are included in the model (see Materials and Methods). Then there is a unique steady state and the homoclinic bifurcation no longer exists. Nevertheless, long-period oscillations are present (Fig. 3 *C*). Importantly, the dependence of the period range of the oscillations on K_{PLC} remains very similar.

We also introduced plasma-membrane fluxes of Ca^{2+} into the negative-feedback model (Fig. 3 *D*). We observed a similar picture as without plasma membrane fluxes, provided that the plasma-membrane fluxes were comparatively moderate. However, when the plasma-membrane Ca^{2+} fluxes are large enough, the effect of IP_3K on the oscillation period practically disappears. In contrast, the period behavior in the positive-feedback model is less affected by changes in the magnitude of the plasma-membrane Ca^{2+} fluxes. To show this, we evaluated the range of oscillation periods $\Delta T = T_{max} - T_{min}$, where T_{max} and T_{min} are the maximal and minimal period that are obtained for low and high stimulation, respectively, for two different strengths of the plasma-membrane Ca^{2+} fluxes ($\varepsilon = 1$ and $\varepsilon = 4$). The positive-feedback model exhibits in both cases a much larger period range than the corresponding model without feedback (Fig. 3 *E*). In contrast, the increase of the period range through negative feedback is only seen when the plasma-membrane Ca^{2+} fluxes are comparatively small, $\varepsilon = 1$ (Fig. 3 *F*).

In summary, both positive and negative feedbacks of Ca^{2+} on IP_3 may serve a physiological role by greatly enhancing the range of frequency encoding of the agonist stimulus. The frequency encoding supported by the positive feedback is more robust against variations in the kinetic parameters of the Ca^{2+} transport processes.

Positive and negative models respond differently to changes in feedback IP_3 turnover time

In the model simulations, we noticed that the characteristic time of IP_3 turnover τ_p has a decisive impact on the Ca^{2+}-IP_3 oscillators. The measured IP_3 turnover times span a relatively wide range, from 0.1 to >10 s depending on cell type and experimental conditions (34,35). We have found that fast IP_3 turnover ($\tau_p \approx 0.1$–2 s) is associated with long oscillation periods in the positive-feedback model. Conversely, the negative-feedback model exhibits long-period oscillations when the IP_3 turnover is comparatively slow ($\tau_p \approx 10$–15 s).

Insight into the origin of this difference between the two models can be gained by looking at the time courses of the model variables. In the positive feedback model, fast IP_3 turnover ($\tau_p = 0.1$ s) yields high-amplitude oscillations in $[Ca^{2+}]_c$ and $[IP_3]$ (Fig. 4 *A*, *solid* and *dashed lines*, respectively). $[Ca^{2+}]_c$ and $[IP_3]$ rise simultaneously, and IP_3-induced Ca^{2+} release and Ca^{2+}-activated IP_3 production coincide. After termination of the $[Ca^{2+}]_c$ spike, $[IP_3]$ returns quickly to a basal level, because Ca^{2+}-activated IP_3 production has ceased and IP_3 degradation is fast. Also, the IP_3Rs close efficiently after the spike (Fig. 4 *A*, *dotted line* showing the fraction of open IP_3R). For slow IP_3 turnover ($\tau_p = 15$ s) $[IP_3]$ does not sufficiently decline after the $[Ca^{2+}]_c$ spike, leading to an increased basal opening of the IP_3R, lower ER Ca^{2+} store loading and, consequently, much less pronounced $[Ca^{2+}]_c$ spikes (Fig. 4 *A*).

Not only the spike characteristics but also the oscillation period and the range of agonist stimuli that give oscillations are affected by the IP_3 half-life. For fast IP_3 turnover, oscillations in the positive-feedback model are observed over a wide range of stimuli (Fig. 4 *C*, $\tau_p = 0.1$ s). Slower IP_3 turnover leads to reduced oscillation ranges and also much smaller amplitudes (Fig. 4 *C*, $\tau_p = 5$ and 15 s). Importantly, also, the capacity for frequency encoding of the stimulus, as measured by the period range of oscillations, is high when the IP_3 turnover is fast (Fig. 4 *E*).

In the negative-feedback model, changing the timescale of IP_3 turnover has the opposite effect. When IP_3 turnover is fast ($\tau_p = 0.1$ s), a rise in $[Ca^{2+}]_c$ triggers, via activation of IP_3K, a pronounced decrease in $[IP_3]$, which in turn limits further Ca^{2+} release (Fig. 4 *B*). Therefore, the $[Ca^{2+}]_c$ spikes are relatively small and $[IP_3]$ shows strong variations (*solid* and *dashed lines*, respectively, in Fig. 4 *B*). When the IP_3 lifetime is larger ($\tau_p = 15$ s), $[IP_3]$ remains at a relatively high level throughout and the $[Ca^{2+}]_c$ spikes are accordingly more pronounced (Fig. 4 *B*). Moreover, for slow IP_3 degradation, the range of stimuli where oscillations occur is larger (Fig. 4 *D*). The capacity for frequency encoding as measured by the range of oscillation periods, ΔT, strongly increases with the IP_3 half-life (Fig. 4 *F*). This finding agrees with the frequent observation that negative feedback is more prone to oscillate when the controlled variable (here IP_3) responds slowly.

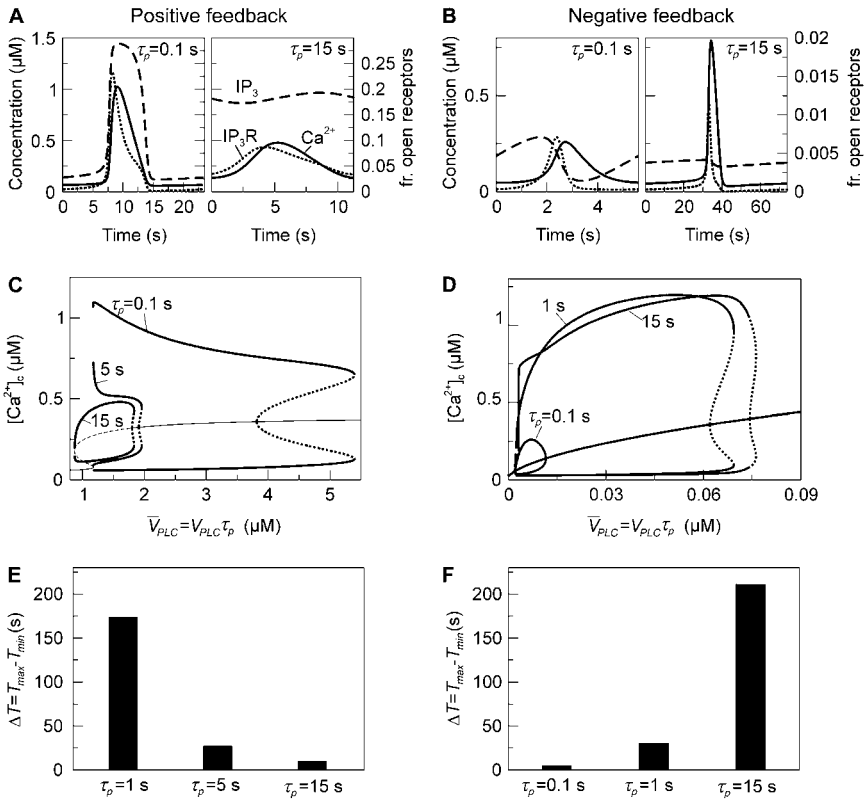

FIGURE 4 IP_3 turnover time controls feedbacks. (*A*) Positive-feedback model. Dynamics of $[Ca^{2+}]_c$, $[IP_3]$, and the fraction of open IP_3Rs (*solid*, *dashed*, and *dot-dashed lines*, respectively) during an oscillation period; the fraction of open IP_3Rs is given by $[rcp/(c+K_a)/(p+K_p)]^3$ (see Eq. 6). Fast IP_3 turnover yields a pronounced spike (*left panel*, $\tau_p = 0.1$ s), whereas slow IP_3 turnover supports only a small-amplitude response (*right panel*, $\tau_p = 15$ s). (*B*) The negative-feedback model shows the opposite behavior, with a small-amplitude response for fast IP_3 turnover (*left panel*, $\tau_p = 0.1$ s) and a sharp spike for slow IP_3 turnover (*left panel*, $\tau_p = 15$ s). (*C*) Positive-feedback model. Bifurcation diagram showing the maxima and minima of the $[Ca^{2+}]_c$ oscillations as a function of the stimulus for different values of the IP_3 turnover. The bifurcation diagrams for different values of τ_p are compared by plotting them against the product $\bar{V}_{PLC} = V_{PLC}\,\tau_p$; in this way, the steady-state concentrations of Ca^{2+} and IP_3 are identical for a given $\bar{V}_{PLC}$ (*solid* and *dashed lines* indicate stable and unstable states, respectively; the stability of the steady state is shown for $\tau_p = 15$ s). Both amplitude and range of stimuli leading to oscillations increase with faster IP_3 turnover. (*D*) The corresponding bifurcation diagrams for the negative-feedback model show the opposite behavior. The amplitude and range of stimuli leading to oscillations increase with slower IP_3 turnover. (*E*, *F*) Dependence of frequency encoding on IP_3 turnover in the positive and negative feedback models, respectively. Shown are the differences ΔT between the largest (for low stimulation) and smallest (for high stimulation) oscillation period.

To summarize, frequency encoding in the two feedback models poses opposite requirements on IP_3 turnover: positive and negative feedbacks are efficient frequency modulators when the IP_3 turnover is fast and slow, respectively. The critical IP_3 lifetimes estimated in the model indicate that both cases could be realized physiologically.

Period control is shared by all processes

The calculations have shown that the inclusion of IP_3 dynamics strongly alters the frequency properties of the oscillator and, particularly, leads to long-period oscillations. We have, therefore, quantified the control of the IP_3 dynamics and the other processes present in the model on the oscillation period. To this end, we have used the following sensitivity measure

$$C_i = \frac{\tau_i}{T}\frac{\partial T}{\partial \tau_i}, \quad \text{for} \quad i = er, pm, p, r, \tag{9}$$

which we refer to as period control coefficients (see also Wolf et al. (42)). The C_i set the change of the oscillation period T in proportion to the change in the characteristic time τ_i of an individual process i. We analyzed the control of the following processes: IP_3 metabolism (with τ_p as defined in Eqs. 3 and 4), the IP_3R dynamics (with τ_r as defined in Eq. 8), Ca^{2+} transport across the ER membrane (achieved by scaling $v_{rel} - v_{serca}$ with $1/\tau_{er} = V_{serca}/K_{serca}$ in Eq. 6), and Ca^{2+} transport across the plasma membrane (achieved by scaling $v_{in} - v_{out}$ with $1/\tau_{pm} = \varepsilon V_{pm}/K_{pm}$ in Eq. 6). A positive period control coefficient implies that a slowing of the respective process (i.e., increase in τ_i) raises the period. At any point, the period control coefficients sum to unity, $C_p + C_r + C_{er} + C_{pm} = 1$, so that each coefficient quantifies the relative contribution of a single process to the oscillation period (43).

The control coefficients were calculated for various levels of stimulation in the positive and negative feedback models. Because these levels correspond to different oscillation periods, we can plot the C_i against the period. Fig. 5, *A* and *B*, depict the result for the model without plasma-membrane fluxes of Ca^{2+} ($\varepsilon = 0$). Positive and negative feedback models yield a similar picture. The control is distributed between the dynamics of IP_3, Ca^{2+}, and IP_3R. In long-period oscillations, the IP_3 turnover has the leading control (*dot-dashed lines*). The IP_3R dynamics contributes more significantly to setting the period of fast oscillations, especially in the positive-feedback model (*dotted lines*).

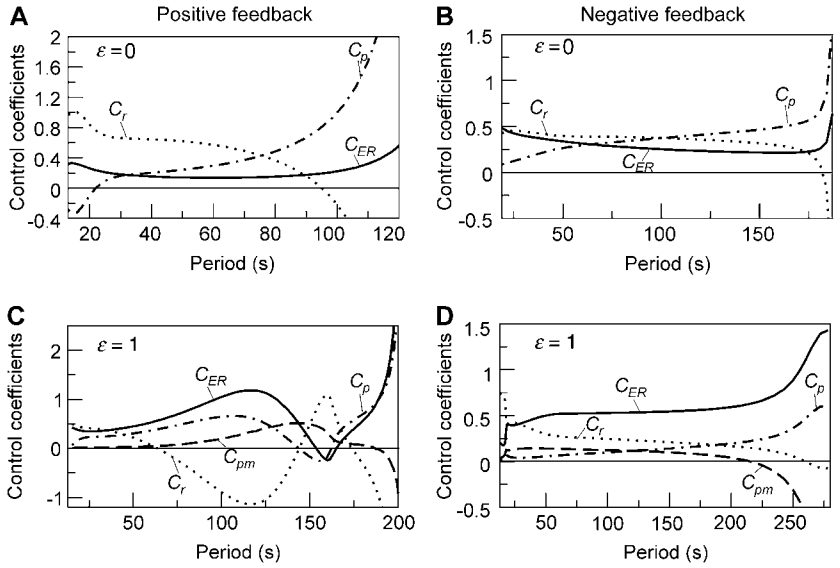

FIGURE 5 Control coefficients for the oscillation period. (*A*, *B*) Positive and negative feedback models, respectively, in the absence of Ca^{2+} fluxes across the plasma membrane ($\varepsilon = 0$); control coefficients of Ca^{2+} exchange across the ER membrane (C_{er}, *solid line*), IP_3 metabolism (C_p, *dashed line*), and IP_3R dynamics (C_r, *dotted line*) as function of the period of the oscillations. A positive period control coefficient signifies that a slowing of the corresponding process increases the oscillation period. (*C*, *D*) Period control coefficients in the positive and negative feedback models, respectively, in the presence of plasma-membrane fluxes of Ca^{2+} ($\varepsilon = 1$). The dash-dotted line indicates the control exerted by Ca^{2+} exchange across the plasma membrane (C_{pm}).

The distribution of control becomes more complex when the plasma-membrane fluxes of Ca^{2+} are included (Fig. 5, *C* and *D*; $\varepsilon = 1$), although, interestingly, the plasma-membrane fluxes exert very little period control themselves (*dashed lines*). There are several notable features. First, the fast oscillations in the positive-feedback model are no longer dominated by the IP_3R dynamics. There is even a rather counterintuitive behavior at intermediate periods where acceleration of the IP_3R dynamics would result in a slowing of the oscillations ($C_r < 0$). Second, the overall tendency that the IP_3 dynamics are more relevant for slow oscillations is preserved. However, the dynamics of ER Ca^{2+} release and refilling now play a more pronounced role in setting the period.

This quantification of period control reveals that no process can be singled out as a unique period controlling factor. Depending on the oscillation mechanism and the reference period, the IP_3 turnover, the ER Ca^{2+} fluxes, and the IP_3R dynamics can all exert strong control.

How to distinguish Ca^{2+} feedbacks on IP_3 metabolism experimentally: model predictions

Our analysis has shown that oscillation mechanisms involving Ca^{2+}-activated PLC or IP_3K are sensitive to the timescale of IP_3. This offers the possibility to experimentally interfere with the oscillation mechanism by perturbing the IP_3 turnover.

The overexpression of IP_3 metabolizing enzymes would accelerate the IP_3 turnover and also decrease $[IP_3]$ (see Eqs. 3–5). Overexpression of either IP_3 5-phosphatase or IP_3 3-kinase can abolish Ca^{2+} and IP_3 oscillations. In the case of IP_3P overexpression, this effect can be revoked by an increase in agonist dose, while quenching of oscillations with overexpression of the Ca^{2+}-dependent IP_3K is predicted to be irreversible. However, positive- and negative-feedback models behave in the same way (see Supplementary Material, Fig. S1).

A different result is obtained if the IP_3 turnover is slowed by introducing IP_3-binding proteins (IP_3 buffer) into the cell. To be specific, we assume a monovalent IP_3 buffer with on- and off-rate constants k_{on} and k_{off}, respectively. The IP_3 balance equation (Eq. 3) is then modified to

$$\frac{dp}{dt} = \frac{1}{\tau_p}(v_{PLC} - v_{deg}) - k_{on}(B - C)p + k_{off}C,$$
$$\frac{dC}{dt} = k_{on}(B - C)p - k_{off}C, \qquad (10a,b)$$

where p as before stands for $[IP_3]$, B denotes the total concentration of the introduced IP_3 buffer, and C is the concentration of occupied IP_3 buffer. If the binding of IP_3 to the buffer is fast compared to the IP_3 degradation rate, the amount of occupied buffer will be in equilibrium with $[IP_3]$. This implies $C = Bp/(K_B + p)$, where $K_B = k_{off}/k_{on}$ is the dissociation constant. Summing Eqs. 10a and 10b, and using the equilibrium relation for C, one obtains for the dynamics of unbound IP_3

$$\frac{dp}{dt} = \frac{1}{\tau_p'}(v_{PLC} - v_{deg}), \qquad (11)$$

with the modified characteristic time of IP_3 turnover

$$\tau_p' = \tau_p\left(1 + \frac{BK_B}{(K_B + p)^2}\right). \qquad (12)$$

The IP_3 buffer creates an additional bound pool of IP_3 that is protected from degradation. Then the buildup of free $[IP_3]$ after PLC activation is delayed, because the buffer binding sites also need to be filled. Similarly, the decay of free $[IP_3]$ is slowed, because IP_3 molecules dissociate from the buffer as cellular $[IP_3]$ decreases. Precisely these two effects are accounted for by the modified time constant τ_p', which

increases with the buffer concentration (Eq. 12). Note that the balance between the rates of IP_3 production and degradation is unaffected by the buffer. In particular, the IP_3 buffer would not change the steady-state concentration of free IP_3 attained when $\nu_{PLC} = const.$. (The endogenous IP_3 binding sites have already been accounted for by the characteristic time of IP_3 turnover, τ_p, defined in the absence of the exogenous IP_3 buffer.)

Introducing an exogenous IP_3 buffer into a core Ca^{2+} oscillator model operating with constant PLC activity and Ca^{2+}-insensitive degradation (such as the model discussed above in the absence of Ca^{2+} feedbacks on IP_3), will delay the rise in $[IP_3]$ after PLC activation. However, eventually the same steady-state concentration of free $[IP_3]$ would be reached as without buffer. Therefore, Ca^{2+} oscillations may set in with an increased latency, whereas spike shape and period would be unaffected by the presence of the IP_3 buffer.)

When introducing the IP_3 buffer into the positive- and negative-feedback models, we find that for low concentrations of IP_3 buffer ($0 < B < 10$ μM for $K_B = 0.13$ μM) the oscillations persist in both models. However, depending on which type of Ca^{2+} feedback is present, IP_3 buffer affects the kinetic properties of the $[Ca^{2+}]_c$ oscillations in very different ways. In the positive-feedback model, the IP_3 buffer slows the Ca^{2+} responses. The rate of $[Ca^{2+}]_c$ rise in an individual spike is predicted to be decreased by the buffer in a dose-dependent manner (Fig. 6 *A*, *solid line*). Another characteristic property of $[Ca^{2+}]_c$ oscillations is the wave speed—the velocity at which a calcium spike propagates through the cell. To evaluate the effect of IP_3 buffer on wave propagation, we added to the model diffusion of Ca^{2+} and IP_3 in the cytoplasm and solved the resulting reaction-diffusion equations numerically on a one-dimensional domain. The propagation speed of a Ca^{2+} spike shows a very similar behavior as the rate of $[Ca^{2+}]_c$ rises: it decreases strongly as a function of IP_3 buffer concentration in the positive-feedback model (Fig. 6 *B*, *solid line*). In contrast, in the negative-feedback model, the IP_3 buffer will cause hardly perceptible increases in the rate of Ca^{2+} rise (Fig. 6 *A*, *dashed line*) and the wave speed (Fig. 6 *B*, *dashed line*). These two properties are well suited for experimental measurements, because they have been found to be remarkably constant in cells not perturbed by IP_3 buffer (44–46).

For higher concentrations of IP_3 buffer ($B > 20$ μM), the differences between the positive- and negative-feedback models are even clearer. In the positive-feedback model, the IP_3 buffer completely abolishes the $[Ca^{2+}]_c$ oscillations, and instead a single slow $[Ca^{2+}]_c$ transient is observed (Fig. 6 *C*). In the negative feedback model, the $[Ca^{2+}]_c$ oscillations persist even for very high concentrations of IP_3 buffer, although the oscillation period is increased (Fig. 6 *D*).

As IP_3 buffering causes the strongest effects in the positive-feedback model, we have analyzed this case in more detail. Fig. 7 *A* summarizes the results by showing the regions of oscillatory behavior as a function of the stimulus (V_{PLC}) and the concentration of exogenous IP_3 buffer. Four different regions can be distinguished. In region I, the IP_3 buffer slows the oscillations with respect to rise time and propagation speed (see *solid lines* in Fig. 6, *A* and *B*). In region II, high enough IP_3 buffer concentrations abolish the

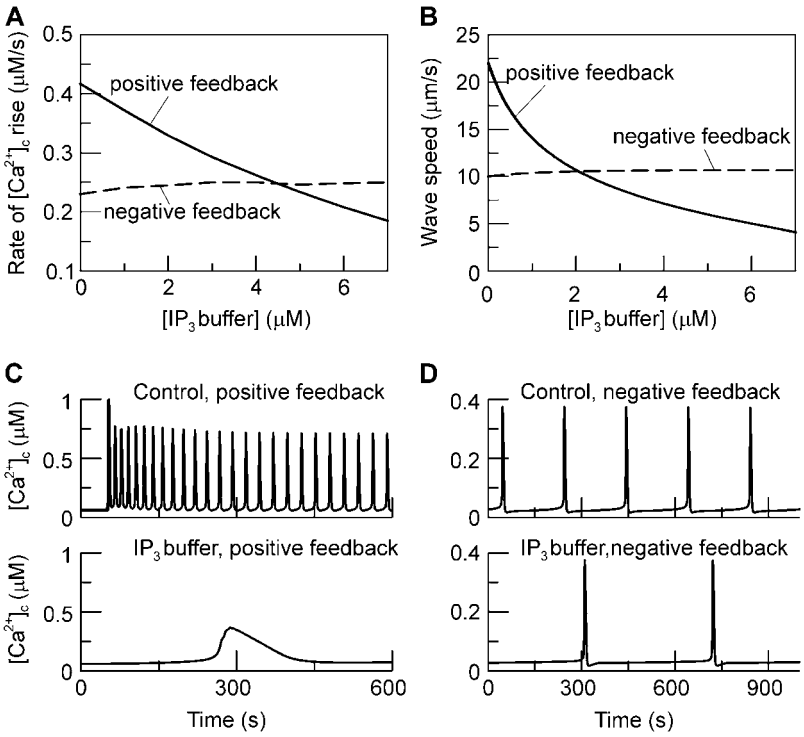

FIGURE 6 Slowing of the IP_3 turnover with an IP_3 buffer. (*A*) The maximal rate of $[Ca^{2+}]_c$ rise during a $[Ca^{2+}]_c$ spike decreases as a function of IP_3 buffer concentration in the positive-feedback model (*solid line*), whereas it is barely affected in the negative-feedback model (*dashed line*). The results are shown for $V_{PLC} = 3$ μM/s (positive feedback) and $V_{PLC} = 0.4$ nM/s (negative feedback); similar results are obtained for other values. (*B*) The intracellular wave speed decreases as a function of IP_3 buffer concentration in the positive-feedback model (*solid line*), whereas it is barely affected in the negative-feedback model (*dashed line*). A solitary Ca^{2+} wave is initiated by a local increase in $[IP_3]$; $[Ca^{2+}]_c$ and $[IP_3]$ diffuse with diffusion constants of 20 and 280 μm^2/s, respectively; $V_{PLC} = 0.976$ μM/s, (positive feedback) and 0.217 nM/s (negative feedback). (*C*) High IP_3 buffer concentration abolishes oscillations in the positive-feedback model ($B = 50$ μM, $V_{PLC} = 1.6$ μM/s). (*D*) Oscillations persist in the presence of IP_3 buffer in the negative feedback model ($B = 50$ μM, $V_{PLC} = 0.6$ nM/s). In all panels the IP_3 buffer dissociation constant is $K_B = K_p = 0.13$ μM. For the positive-feedback calculations: $\varepsilon = 2$, $\tau_p = 1$ s, $\tau_r = 6$ s, $v_0 = 0.002$ μM/s, $\phi = 0.001$/s. For the negative-feedback model $\varepsilon = 0.1$. Other parameters are as listed in Table 1.

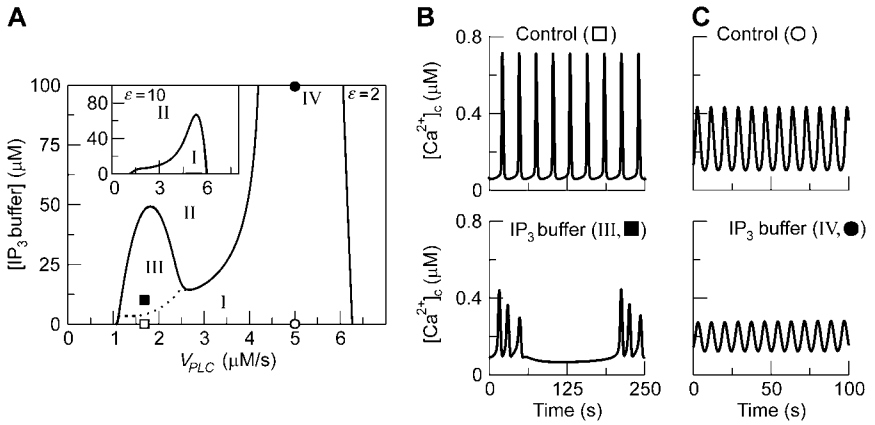

FIGURE 7 Complex responses to an IP_3 buffer in the positive-feedback model. (*A*) Bifurcation diagram showing the region of oscillations as function of stimulus (V_{PLC}) and IP_3 buffer concentration (*gray-shaded area*; the *solid lines* indicate the locus where the steady state becomes unstable via a Hopf bifurcation). In region I, regular oscillations have a decreased rate of $[Ca^{2+}]_c$ rise with increased [IP_3 buffer] as shown in Fig. 6 *A*. In region II, the IP_3 buffer abolishes the Ca^{2+} oscillations completely, as shown in Fig. 6 *C*. In region III, bursting $[Ca^{2+}]_c$ oscillations are observed (the lower boundary of this region is determined by a period doubling bifurcation, *dotted line*). We have indicated an additional region IV, which is characterized by oscillations persisting even at high [IP_3 buffer]. The parameters are as in Fig. 6, with $\varepsilon = 2$. When the strength of the Ca^{2+} plasma-membrane fluxes is increased ($\varepsilon = 10$), regions III and IV disappear (*inset*). (*B*) Example of bursting oscillations observed in region III (*top panel*, control without IP_3 buffer; *bottom panel*, [IP_3 buffer] = 10 μM; V_{PLC} = 1.6 μM/s). (*C*) Example of oscillations in region IV (V_{PLC} = 5 μM/s; [IP_3 buffer] = 100 μM), which are characterized by high frequency and low amplitude.

oscillations (shown in Fig. 6 *C*). In region III, IP_3 buffer can cause more complex oscillations, such as the bursting oscillations shown in Fig. 7 *B*. For a large range of stimuli, the oscillations disappear when sufficiently high amounts of IP_3 buffer are added (transition into region II). However for strong stimulation, there can be an additional domain, region IV (Fig. 7 *A*). Here, the oscillations persist even at very high IP_3 buffer concentration but have strongly diminished amplitude (Fig. 7 *C*). Note that in the presence of sufficiently high IP_3 buffer, only fast oscillations (at high stimulation) can be retained. The long-period oscillations, which depend on Ca^{2+} feedback on PLC are invariably abolished by the IP_3 buffer.

Whether regions III and IV exist, depends on the kinetic parameters of the Ca^{2+} fluxes. The inset in Fig. 7 *A* shows a situation where the Ca^{2+} fluxes across the plasma membrane were increased fivefold. Then only regions I and II remain, and sufficiently high buffering of IP_3 always suppresses oscillations. Closer analysis revealed that if the system can oscillate for constant [IP_3] then IP_3 buffer never completely abolish the oscillations and a region IV exists (A. Politi, unpublished data).

Expression of an IP_3 buffer suppresses Ca^{2+} oscillations

The most significant difference in the responses of the positive-feedback and negative-feedback models to the IP_3 buffer is that agonist-induced oscillations always persist in the latter model whereas they can be abolished in the former. To examine the model predictions experimentally, we took advantage of a molecular IP_3 buffer developed in our laboratory, which consists of the N-terminal ligand binding domain of rat type 1 IP_3R linked to enhanced green fluorescent protein (EGFP-LBD; (47); L. Gaspers, P. Burnett, J. Johnston, A. Politi, T. Höfer, S. Joseph and A. Thomas, unpublished data). CHO cells were transiently transfected with EGFP or EGFP-LBD then challenged with submaximal and maximal ATP concentrations. The subsequent $[Ca^{2+}]_c$ responses were monitored via changes in the fura-2 fluorescence ratio. EGFP fluorescence was utilized to distinguish transfected from nontransfected cells in a given field of view and to estimate the intracellular concentration of the transgene (see Materials and Methods).

The addition of low ATP concentrations elicited periodic $[Ca^{2+}]_c$ spikes in >85% of the CHO cells expressing EGFP (Fig. 8, *A* and *B*) or nonexpressing cells from cultures transfected with EGFP-LBD (not shown). Agonist-evoked $[Ca^{2+}]_c$ oscillations required functional ER Ca^{2+} stores (i.e., they were thapsigargin-sensitive), but ceased abruptly upon removing extracellular Ca^{2+} suggesting that plasma membrane Ca^{2+} fluxes are relatively strong in this cell type (not shown). In both GFP-expressing and nonexpressing cells, the $[Ca^{2+}]_c$ increase immediately after agonist challenge was more prolonged and the rate of Ca^{2+} rise faster than subsequent $[Ca^{2+}]_c$ oscillations (Fig. 8, *A* and *C*). No systematic differences were evident in agonist sensitivity or the pattern of the $[Ca^{2+}]_c$ spiking between EGFP expressing and nonexpressing cells suggesting that neither EGFP nor the transfection reagents per se had significant effects on Ca^{2+} signaling. By contrast, the presence of EGFP-LBD had a dose-dependent effect on the agonist-dependent Ca^{2+} oscillations in CHO cells (Fig. 8 *A*). High levels of EGFP-LBD expression correlated with a loss of repetitive $[Ca^{2+}]_c$ spiking and the appearance of low amplitude $[Ca^{2+}]_c$ increases (Fig. 8, *A* and *B*). Moreover, EGFP-LBD expression significantly slowed the rate of $[Ca^{2+}]_c$ rise (Fig. 8 *C*; $p < 0.01$) and significantly broadened the width of the $[Ca^{2+}]_c$ spike (Fig. 8 *D*; $p < 0.05$) compared to EGFP expressing cells. For these data, we only analyzed EGFP-LBD expressing cells where low ATP challenge (0.5 or 1 μM) evoked at least three sequential baseline-separated Ca^{2+} spikes. This was observed predominately in cells expressing low levels of EGFP-LBD and, thus we probably underestimated the actions of IP_3 buffering on the kinetics of $[Ca^{2+}]_c$ oscillations.

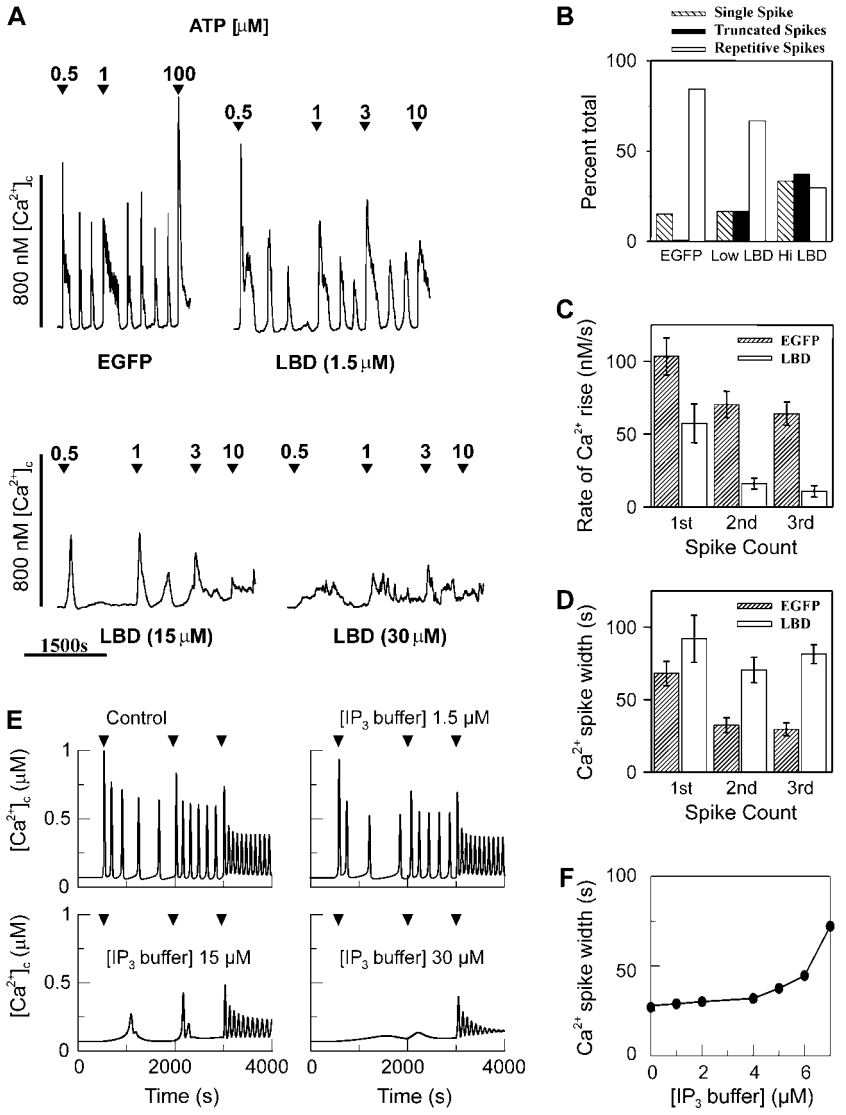

FIGURE 8 The effects of a molecular IP_3 buffer on ATP-evoked $[Ca^{2+}]_i$ oscillations in CHO cells. CHO cells ($n = 5$ independent cultures) were transiently transfected with pEGFP-LBD (EGFP-LBD) or pEGFP-C1 (EGFP). The cells were loaded with fura-2/AM 16–48 h posttransfection and challenged with the indicated ATP concentrations. The traces (*A*) show typical ATP-evoked $[Ca^{2+}]_c$ spikes in CHO cells transiently expressing EGFP or different levels of EGFP-LBD. The intracellular EGFP-LBD concentration was estimated as described in Materials and Methods. (*B*) Data show the effects of increasing EGFP-LBD expression on ATP-evoked Ca^{2+}signals. CHO cells expressing EGFP-LBD were arbitrarily divided into low (489 ± 66 units; $n = 18$ cells) or high (3170 ± 480 units; $n = 27$ cells) categories using a cutoff of 1000 fluorescence intensity units. The estimated mean EGFP-LBD concentration was 6 ± 0.8 or 38 ± 6 μM, respectively. The mean EGFP fluorescence intensity was 7400 ± 615 units (89 ± 7 μM; $n = 198$ cells). Truncated spikes are defined as low amplitude $[Ca^{2+}]_c$ oscillations similar to those shown in the bottom traces of panel *A*. The initial rates of $[Ca^{2+}]_c$ rise (*C*) and the widths of the $[Ca^{2+}]_i$ spike (*D*) were calculated in cells expressing EGFP ($n = 52$ cells) or EGFP-LBD ($n = 20$ cells) where ATP challenge (0.5 or 1 μM) evoked at least three sequential baseline-separated Ca^{2+} spikes. The width of the $[Ca^{2+}]_c$ spike were determined at half-peak height. (*E*) The positive feedback model, Ca^{2+} activation of PLC, with different IP_3 buffer concentrations (as indicated) shows a good agreement with the EGFP-LBD experimental data shown in panel *A*. An increase in ATP is simulated by an increase in the maximal activity of PLC (*arrowheads*). (*F*) In the positive feedback model we also observe a significant increase in spike width (calculated at half-peak height). To match the Ca^{2+} oscillations in CHO cells all variables have been slowed by a factor 10, reference parameter set as in Fig. 6 $\varepsilon = 10$. In panel *E*, $V_{PLC} = 0.125$, 0.2, 0.4 μM/s. Initial condition at V_{PLC}=0.05 μM/s. In panel *F*, V_{PLC}=0.2 μM/s.

According to the theoretical results, the disappearance of the oscillations and a slowing of the Ca^{2+} rise suggests that IP_3 oscillations driven by positive feedback of Ca^{2+} on IP_3 production are involved in this system. We have simulated the positive-feedback model with relatively strong plasma-membrane Ca^{2+} fluxes as observed in CHO cells. At high concentrations of IP_3 buffer (Fig. 8 *E*), the model exhibits single transients (for lower agonist dose), and repetitive truncated spikes (for high agonist dose). Both responses closely resemble the experimentally observed patterns in cells expressing high amounts of EGFP-LBD. The Ca^{2+} oscillations at lower concentrations of IP_3 buffer (Fig. 8 *F*) exhibit a broadening of the individual spikes, which is very similar to the experimental observation in cells expressing low amounts of EGFP-LBD. Also the observed decrease of the rate of Ca^{2+} rise is reproduced by the model (data similar to Fig. 6 *A*). A model with negative feedback could account for none of the experimental findings (see Fig. 6).

DISCUSSION

There has been increasing evidence that hormone-evoked periodic Ca^{2+} spiking can be accompanied by oscillations of the Ca^{2+}-releasing second messenger IP_3 (12–15). The experimental findings raise the questions of i), the underlying mechanisms of IP_3 oscillations and ii), their potential functional role. The theoretical analysis and experiments presented here provide insight into both issues.

Several processes could be involved in the generation of IP_3 oscillations. Feedbacks of IP_3 and the second product of the PLC reaction, diacylglycerol, on PLC and upstream agonist receptor/G-protein could produce IP_3 oscillations without involvement of Ca^{2+} (26,48). Alternatively, feedbacks

on IP_3 metabolism may be mediated by Ca^{2+}, resulting in coupled IP_3-Ca^{2+} oscillators (27,30,32,49). In this work, we have focused on the latter type of feedback oscillators because they can naturally account for the experimental observations of i), Ca^{2+} oscillations at clamped IP_3 concentration and ii), coupled IP_3 and Ca^{2+} oscillations. We considered prototypical positive and negative feedbacks of Ca^{2+} ions on IP_3 metabolism: Ca^{2+} activation of PLC and Ca^{2+} activation of IP_3 3-kinase, respectively.

The incorporation of such feedbacks into a core Ca^{2+} oscillator model based on the regulatory properties of the IP_3 receptor can greatly expand the sensitivity of signal transduction to the hormonal stimulus. The presence of either feedback increases the range of agonist concentrations where one observes Ca^{2+} oscillations and enhances the ability to frequency-encode the agonist dose. Thus Ca^{2+} feedbacks on IP_3 metabolism represent a possible mechanism for the generation of robust long-period oscillations. This is likely to be an important component of frequency-modulated Ca^{2+} signals, because physiological responses are controlled in this lower frequency range (50,51). Thus our model points to a physiological role of IP_3 oscillations.

For the positive feedback to modulate the oscillation properties, the Ca^{2+} sensitivity of PLC needs to be only somewhat above basal $[Ca^{2+}]_c$ (K_{PLC} =0.1–0.2 μM). Such values are in agreement with experimental data (33). This feedback delays the onset of the Ca^{2+} spike, because both $[IP_3]$ and $[Ca^{2+}]_c$ must rise to a certain level for triggering explosive opening of the IP_3R. In this way, long oscillation periods arise for low levels of stimulation, whereas for strong stimuli the high IP_3 level obviates the need for additional Ca^{2+} activation of PLC. We have here specifically assumed that Ca^{2+} and agonist act on the same isoform of PLC (e.g., PLCβ). However, similar results were obtained in a model variant when the isoform PLCδ is also included in the model, which is a Ca^{2+}-sensitive but agonist-insensitive PLC isoform (results not shown).

Negative feedback exerts control on the Ca^{2+} oscillations when IP_3 removal takes place predominantly via IP_3K rather than by the IP_3P (>60% of the removal flux at high $[Ca^{2+}]_c$ carried by IP_3K). Long oscillation periods are generated when $[IP_3]$ drops in the wake of a Ca^{2+} spike due to IP_3K activation and subsequently recovers slowly to the level needed to activate the IP_3R. We have found that this mechanism requires a finely tuned interplay between IP_3 metabolism and Ca^{2+} fluxes. This sensitivity may explain the discrepancy to the work of Dupont and Erneux (32), who reported only small effects of IP_3K on $[Ca^{2+}]_c$ oscillation periods. In contrast, the effects of the positive feedback were found to be robust with respect to the properties of the core Ca^{2+} oscillator.

The different modes of action of positive and negative feedbacks are reflected by opposing requirements on the lifetime of IP_3. In the case of positive feedback, IP_3 turnover must be fast to support long-period oscillations, allowing for i), coincidence of Ca^{2+} and IP_3 spikes and ii), for the rapid removal of IP_3 in the wake of a spike. In the case of negative feedback, slow IP_3 turnover is required for the slow recovery of IP_3 levels in between spikes. In different cellular systems, either one of the IP_3 feedbacks could play a significant role in controlling Ca^{2+} oscillations, depending primarily on the underlying turnover rate of IP_3. However, they cannot be expected to act synergistically.

A critical question is the experimental identification of the mechanisms that drive IP_3 oscillations. The theoretical analysis showed that slowing the IP_3 turnover by means of an IP_3 buffer can be used to distinguish between the two feedback mechanisms. An IP_3 buffer can quench the oscillations generated by an IP_3-Ca^{2+} oscillator based on positive feedback of Ca^{2+} on IP_3, but not by one based on negative feedback. Our preliminary modeling results indicate that the weak response of the negative-feedback oscillator to IP_3 buffering could be a general property not limited to a mechanism operating through IP_3 3-kinase. We obtained very similar results with an alternative mechanism acting through PKC-dependent inactivation of the agonist receptors.

To test this theoretical prediction, we overexpressed the ligand binding domain of the type 1 IP_3R in a mammalian cell line, which acts as an IP_3 buffer. The observed dose-dependent suppression of Ca^{2+} oscillations demonstrates that the IP_3 dynamics play a critical role in the oscillator mechanism. Moreover, the detailed agreement between the experimental data and the simulations of the positive-feedback model is consistent with a coupled IP_3-Ca^{2+} oscillator based on Ca^{2+} activation of PLC.

SUPPLEMENTARY MATERIAL

An online supplement to this article can be found by visiting BJ Online at http://www.biophysj.org.

We thank Dr. Fang Lui for technical assistance with the CHO cell cultures, Dr. Suresh Joseph (Thomas Jefferson University) for supplying cDNA encoding type 1 LBD, and Paul Burnett for constructing the EGFP-LBD plasmid.

Support by the Boehringer Ingelheim Fonds (to A.P.), the Hepatocyte Systems Biology program of the Federal Ministry for Education and Research of German (to T.H.), and United States National Institutes of Health grants DK38422 and AA014918 (to A.P.T.) are gratefully acknowledged.

REFERENCES

1. Rooney, T., E. Sass, and A. P. Thomas. 1989. Characterization of cytosolic calcium oscillations induced by phenylephrine and vasopressin in single fura-2-loaded hepatocytes. *J. Biol. Chem.* 264:17131–17141.
2. Bezprozvanny, I., and B. E. Ehrlich. 1995. The inositol 1,4,5-trisphosphate ($InsP_3$) receptor. *J. Membr. Biol.* 145:205–216.
3. Hajnoczky, G., and A. P. Thomas. 1997. Minimal requirements for calcium oscillations driven by the IP_3 receptor. *EMBO J.* 16: 3533–3543.

4. Marchant, J. S., and C. W. Taylor. 1998. Rapid activation and partial inactivation of inositol trisphosphate receptors by inositol trisphosphate. *Biochemistry*. 37:11524–11533.
5. Yule, D. I., S. V. Straub, and J. I. Bruce. 2003. Modulation of Ca^{2+} oscillations by phosphorylation of Ins(1,4,5)P_3 receptors. *Biochem. Soc. Trans.* 31:954–957.
6. Keizer, J., Y. X. Li, S. Stojilkovic, and J. Rinzel. 1995. $InsP_3$-induced Ca^{2+} excitability of the endoplasmic reticulum. *Mol. Biol. Cell.* 6:945–951.
7. Dupont, G., S. Swillens, C. Clair, T. Tordjmann, and L. Combettes. 2000. Hierarchical organization of calcium signals in hepatocytes: from experiments to models. *Biochim. Biophys. Acta.* 1498:134–152.
8. Schuster, S., M. Marhl, and T. Höfer. 2002. Modelling of simple and complex calcium oscillations. From single-cell responses to intercellular signaling. *Eur. J. Biochem.* 269:1333–1355.
9. Sneyd, J., K. Tsaneva-Atanasova, J. I. Bruce, S. V. Straub, D. R. Giovannucci, and D. I. Yule. 2003. A model of calcium waves in pancreatic and parotid acinar cells. *Biophys. J.* 85:1392–1405.
10. Falcke, M. 2003. On the role of stochastic channel behavior in intracellular Ca^{2+} dynamics. *Biophys. J.* 84:42–56.
11. Marhl, M., T. Haberichter, M. Brumen, and R. Heinrich. 2000. Complex calcium oscillations and the role of mitochondria and cytosolic proteins. *Biosystems.* 57:75–86.
12. Hirose, K., S. Kadowaki, M. Tanabe, H. Takeshima, and M. Lino. 1999. Spatiotemporal dynamics of inositol 1,4,5-trisphosphate that underlies complex Ca^{2+} mobilization patterns. *Science.* 284:1527–1530.
13. Nash, M. S., K. W. Young, R. A. Challiss, and S. R. Nahorski. 2001. Intracellular signalling. Receptor-specific messenger oscillations. *Nature.* 413:381–382.
14. Young, K. W., M. S. Nash, R. A. Challiss, and S. R. Nahorski. 2003. Role of Ca^{2+} feedback on single cell inositol 1,4,5-trisphosphate oscillations mediated by G-protein-coupled receptors. *J. Biol. Chem.* 278:20753–20760.
15. Thore, S., O. Dyachock, and A. Tengholm. 2004. Oscillations of phospholipase C activity triggered by depolarization and Ca^{2+} influx in insulin-secreting cells. *J. Biol. Chem.* 19:19396–19400.
16. Rhee, S. G. 2001. Regulation of phosphoinositide-specific phospholipase C. *Annu. Rev. Biochem.* 70:281–312.
17. Harootunian, A. T., J. P. Kao, S. Paranjape, and R. Y. Tsien. 1991. Generation of calcium oscillations in fibroblasts by positive feedback between calcium and IP_3. *Science.* 251:75–78.
18. Rebecchi, M. J., and S. N. Pentyala. 2000. Structure, function, and control of phosphoinositide-specific phospholipase C. *Physiol. Rev.* 80: 1291–1335.
19. Venance, L., N. Stella, J. Glowinski, and C. Giaume. 1997. Mechanism involved in initiation and propagation of receptor-induced intercellular calcium signaling in cultured rat astrocytes. *J. Neurosci.* 17:1981–1992.
20. Höfer, T., L. Venance, and C. Giaume. 2002. Control and plasticity of intercellular calcium waves in astrocytes: a modeling approach. *J. Neurosci.* 22:4850–4859.
21. Wagner, J., C. P. Fall, F. Hong, C. E. Sims, N. L. Allbritton, R. A. Fontanilla, I. I. Moraru, L. M. Loew, and R. Nuccitelli. 2004. A wave of IP_3 production accompanies the fertilization Ca^{2+} wave in the egg of the frog, Xenopus laevis: theoretical and experimental support. *Cell Calcium.* 35:433–447.
22. Dupont, G., and R. Dumollard. 2004. Simulation of calcium waves in ascidian eggs: insights into the origin of the pacemaker sites and the possible nature of the sperm factor. *J. Cell Sci.* 117:4313–4323.
23. Communi, D., V. Vanweyenberg, and C. Erneux. 1997. D-myo-inositol 1,4,5-trisphosphate 3-kinase A is activated by receptor activation through a calcium: calmodulin-dependent protein kinase II phosphorylation mechanism. *EMBO J.* 16:1943–1952.
24. Woodring, P. J., and J. C. Garrison. 1997. Expression, purification, and regulation of two isoforms of the inositol 1,4,5-trisphosphate 3-kinase. *J. Biol. Chem.* 272:30447–30454.
25. Nalaskowski, M. M., and G. W. Mayr. 2004. The families of kinases removing the Ca^{2+} releasing second messenger Ins(1,4,5)P_3. *Curr. Mol. Med.* 4:277–290.
26. Cuthbertson, K. S., and T. R. Chay. 1991. Modelling receptor-controlled intracellular calcium oscillators. *Cell Calcium.* 12:97–109.
27. Meyer, T., and L. Stryer. 1988. Molecular model for receptor-stimulated calcium spiking. *Proc. Natl. Acad. Sci. USA.* 85:5051–5055.
28. Wakui, M., B. V. Potter, and O. H. Petersen. 1989. Pulsatile intracellular calcium release does not depend on fluctuations in inositol trisphosphate concentration. *Nature.* 339:317–320.
29. Marchant, J. S., and I. Parker. 2001. Role of elementary Ca(2+) puffs in generating repetitive Ca(2+) oscillations. *EMBO J.* 20:65–76.
30. DeYoung, G. W., and J. Keizer. 1992. A single-pool inositol 1,4,5-trisphosphate-receptor-based model for agonist-stimulated oscillations in Ca^{2+} concentration. *Proc. Natl. Acad. Sci. USA.* 89:9895–9899.
31. Dupont, G., O. Koukoui, C. Clair, C. Erneux, S. Swillens, and L. Combettes. 2003. Ca^{2+} oscillations in hepatocytes do not require the modulation of $InsP_3$ 3-kinase activity by Ca^{2+}. *FEBS Lett.* 534: 101–105.
32. Dupont, G., and C. Erneux. 1997. Simulations of the effects of inositol 1,4,5-trisphosphate 3-kinase and 5-phosphatase activities on Ca^{2+} oscillations. *Cell Calcium.* 22:321–331.
33. Blank, J. L., A. H. Ross, and J. H. Exton. 1991. Purification and characterization of two G-proteins that activate the beta-1 isozyme of phosphoinositide-specific phospholipase C. *J. Biol. Chem.* 266:18206–18216.
34. Fink, C. C., B. Slepchenko, I. I. Moraru, J. Schaff, J. Watras, and L. M. Loew. 1999. Morphological control of inositol-1,4,5-trisphosphate-dependent signals. *J. Cell Biol.* 412:929–935.
35. Sims, C. E., and N. L. Allbritton. 1998. Metabolism of inositol 1,4,5-trisphosphate and inositol 1,3,4,5-tetrakisphosphate by the oocytes of Xenopus laevis. *J. Biol. Chem.* 273:4052–4058.
36. Li, Y. X., and J. Rinzel. 1994. Equations for $InsP_3$ receptor-mediated $[Ca^{2+}]_i$ oscillations derived from a detailed kinetic model: a Hodgkin-Huxley like formalism. *J. Theor. Biol.* 166:461–473.
37. Lytton, J., M. Westlin, S. E. Burk, G. E. Shull, and D. H. MacLennan. 1992. Functional comparisons between isoforms of the sarcoplasmic or endoplasmic reticulum family of calcium pumps. *J. Biol. Chem.* 267: 14483–14489.
38. Camello, P., J. Gardner, O. H. Petersen, and A. V. Tepikin. 1996. Calcium dependence of calcium extrusion and calcium uptake in mouse pancreatic acinar cells. *J. Physiol.* 490:585–593.
39. Doedel, E. J. 1981. AUTO, a program for the automatic bifurcation analysis of autonomous systems. *Cong. Numer.* 30:265–384.
40. Boehning, D., and S. K. Joseph. 2000. Direct association of ligand-binding and pore domains in homo- and heterotetrameric inositol 1,4,5-trisphosphate receptors. *EMBO J.* 19:5450–5459.
41. Sneyd, J., K. Tsaneva-Atanasova, D. I. Yule, J. L. Thompson, and T. J. Shuttleworth. 2004. Control of calcium oscillations by membrane fluxes. *Proc. Natl. Acad. Sci. USA.* 101:1392–1396.
42. Wolf, J., S. Becker-Weimann, and R. Heinrich. 2005. Analysing the robustness of cellular rhythms. *Syst. Biol.* 2:35–41.
43. Heinrich, R., and S. Schuster. 1996. The Regulation of Cellular Systems. Chapman and Hall, New York.
44. Thomas, A. P., D. C. Renard, and T. A. Rooney. 1991. Spatial and temporal organization of calcium signalling in hepatocytes. *Cell Calcium.* 12:111–126.
45. Rooney, T. A., E. J. Sass, and A. P. Thomas. 1990. Agonist-induced cytosolic calcium oscillations originate from a specific locus in single hepatocytes. *J. Biol. Chem.* 265:10792–10796.
46. Robb-Gaspers, L. D., and A. P. Thomas. 1995. Coordination of Ca^{2+} signaling by intercellular propagation of Ca^{2+} waves in the intact liver. *J. Biol. Chem.* 270:8102–8107.
47. Gaspers, L. D., and A. P. Thomas. 2005. Calcium signaling in liver. *Cell Calcium.* 38:329–342.

48. Hisatsune, C., K. Nakamura, Y. Kuroda, T. Nakamura, and K. Mikoshiba. 2005. Amplification of Ca^{2+} signaling by diacylglycerol-mediated inositol 1,4,5-trisphosphate production. *J. Biol. Chem.* 280: 11723–11730.

49. Kummer, U., L. F. Olsen, C. J. Dixon, A. K. Green, E. Bornberg-Bauer, and G. Baier. 2000. Switching from simple to complex oscillations in calcium signaling. *Biophys. J.* 79:1188–1195.

50. Hajnoczky, G., L. D. Robb-Gaspers, M. B. Seitz, and A. P. Thomas. 1995. Decoding of cytosolic calcium oscillations in the mitochondria. *Cell.* 82:415–424.

51. Dolmetsch, R. E., R. S. Lewis, C. C. Goodnow, and J. I. Healy. 1997. Differential activation of transcription factors induced by Ca^{2+} response amplitude and duration. *Nature.* 386:855–858.

52. Mak, D. D., S. McBride, and J. K. Foskett. 2001. Regulation by Ca^{2+} and inositol 1,4,5-trisphosphate ($InsP_3$) of single recombinant type 3 $InsP_3$ receptor channels. Ca^{2+} activation uniquely distinguishes types 1 and 3 $InsP_3$ receptors. *J. Gen. Physiol.* 117:435–446.

53. Ramos-Franco, J., M. Fill, and G. A. Mignery. 1998. Isoform-specific function of single inositol 1,4,5-trisphosphate receptor channels. *Biophys. J.* 75:834–839.